Two-Dimensional Flow and NO$_x$ Emissions in Deflagrative Internal Combustion Wave Rotor Configurations

K. Pekkan
Post Doctoral Fellow

M. R. Nalim
Assistant Professor

Mechanical Engineering Department,
Purdue School of Engineering and Technology,
Indiana University–Purdue University
Indianapolis,
723 West Michigan Street,
Indianapolis, IN 46202

A wave rotor is proposed for use as a constant volume combustor. A novel design feature is investigated as a remedy for hot gas leakage, premature ignition, and pollutant emissions that are possible in this class of unsteady machines. The base geometry involves fuel injection partitions that allow stratification of fuel/oxidizer mixtures in the wave rotor channel radially, enabling pilot ignition of overall lean mixture for low NO$_x$ combustion. In this study, available turbulent combustion models are applied to simulate approximately constant volume combustion of propane and resulting transient compressible flow. Thermal NO production histories are predicted by simulations of the STAR-CD code. Passage inlet/outlet/wall boundary conditions are time-dependent, enabling the representation of a typical deflagrative internal combustor wave rotor cycle. Some practical design improvements are anticipated from the computational results. For a large number of derivative design configurations, fuel burn rate, two-dimensional flow and emission levels are evaluated. The sensitivity of channel combustion to initial turbulence levels is evaluated. [DOI: 10.1115/1.1586315]

Introduction

A wave rotor machine utilizes nonsteady wave motion to exchange energy by direct work action between chemically reacting or inert fluids. It consists of a large number of straight channels arranged about the axis of a rotor. By rotation the channel ends are periodically ported to connected steady-flow components. The rotation speed of the rotor is low compared to conventional turbomachines. For detailed descriptions of wave-rotor principles and applications see [1,2]. In this study it is assumed that an internal combustion wave rotor (ICWR) is coupled to a compressor and turbine, which are placed at its inlet and outlet, respectively.

Previous simulations of wave rotor processes have provided good overall indications of wave rotor behavior and performance potential. One-dimensional simulations modeled most loss mechanisms, heat transfer, and combustion in a simplified manner, [3,4,5]. Two-dimensional laminar computations included duct flows, and identified major flow features that influence performance and thermal loads, [6]. An invicid three-dimensional study with rotation can be found in [7]. Feasible modes of combustion wave rotors have been assessed and one-dimensional simulations of basic cycle designs have been performed, [8,9]. Ignition and flame propagation in a wave-rotor-like channel has been experimentally demonstrated, [10]. These studies indicate that it is feasible to design combustion wave rotors with reasonable size and fuel-rate for most gas turbine applications, resulting in pressure gain with lower weight and simpler integration than pressure-exchange wave rotors.

Two major questions that must now be addressed are pollutant emissions of such a system, and the thermal loads on the rotor and other components. Numerical studies of a stratified-charge combustion wave rotor indicate that hot gas leakage and thermal gradients/loads may be a significant problem, [9]. For the pressure-exchange wave-rotor cycle designed for gas turbine top-ping, the one-dimensional and two-dimensional estimates of wall and exit temperatures apparently disagree, creating uncertainty about thermal loads, [6,11]. In general, among remaining challenges affecting the performance of wave rotor machines are: leakage, internal heat transfer, hot gas and air mixing in channels, loss of total pressure at inlet and exit openings, and complex ducting.

One-dimensional gas dynamics codes developed for wave rotor calculations are popular and practical for cycle design, [5], preliminary analysis, and system/component matching, [12]. They are also used to determine the relative importance and sensitivity responses of various design parameters. Both off-design, [13,14], and periodic steady-state studies can be performed with these codes, and key physical phenomena can be modeled with satisfactory accuracy, except for heat transfer and combustion. Models exist for viscous losses, partial opening, leakage, [11], and stratified combustion, [9]. Nevertheless, multi-dimensional simulations are now needed to provide essential flow details and offer a necessary tool for the analysis of some new design ideas. Such simulations are still expensive, partly because transient codes are required. Requirements for refined meshes near turbulent boundary layers and traveling discontinuities (shock and expansion waves, detonations) results in very small time steps and considerable computer time to obtain a complete cycle simulation. Therefore, this study provides two-dimensional flow analysis, focusing on different and improved combustion models, to elaborate and verify previous one-dimensional studies and lead to a simple two-dimensional cycle design approach.

More specifically, this study is aimed at investigating a special feature proposed for combustion wave rotors, which necessitates multi-dimensional analysis. A simple method of pilot ignition aids initiation of a delflagrative or detonative combustion process while allowing for lean-burn, and simultaneously reducing the leakage of hot combustion gases and thermal load on the internal surfaces of a combustion wave rotor. The method consists of creating precise circumferential partition walls in the inlet duct and, as importantly, in the wave rotor channel itself. Note that the use of radial partition walls in the inlet duct has been previously described, [9]. Such partition walls provided circumferential varia-

Copyright © 2003 by ASME
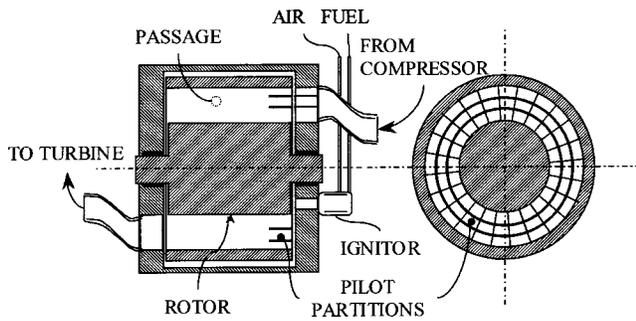
Fig. 1 Internal combustion wave rotor (ICWR) with pilot partition walls

Fig. 2 Internal combustor wave rotor with longitudinal stratification: Developed ("unrolled") view and basic wave dynamics. Refer to Table 1 for phase number descriptions.

tion in the fuel distribution in the inlet, and allow a longitudinally stratified fuel-air mixture to be introduced into the wave rotor channels. This provides ignitable mixtures near the ignition location, and combustible conditions in the remaining mixture.

The use of circumferential partition walls in the current study provides stratification in the radial direction, adding a new level of control of the combustion process. In combination, the partition walls provide a limited region of the channel to be charged with a near-stoichiometric or enriched mixture that ensures ignition or initiation of a deflagrative or detonative combustion process. Similar to pilot combustion in various combustion engines, the enrichment may be with fuel, oxidant, or both. The combustion in this region is controlled by the provision of circumferential partition walls in the rotor channels that extend a relatively short distance into the length of the channel. Figure 1 shows a wave rotor with circumferential partitions near the inlet. The inlet duct partitions can be both circumferential and radial, with different fuel distribution schemes in selected inlet zones.

The significance of the new partitions is multifold; first, it provides for a pilot ignition zone that can be charged by an enriched mixture and separately ignited. This allows for the remaining mixture to be made significantly leaner in fuel than otherwise possible and therefore lower in nitrogen oxide (NO_x) emissions. Second, it provides a noncombustible gas to be placed adjacent to the hub and shroud, thus eliminating the leakage of hot gas from the inlet side of the rotor, and helping to cool the rotor. This will minimize thermal damage of the bearings and other components of the wave rotor, and provide some control of the rotor temperature and its gradient. Third, the most readily ignited mixture is supplied only to the central section, and it avoids pre-ignition by hot gas leaking into the low-pressure inflowing mixture. Fourth, there may be structural advantages as envisaged by Kentfield [15], but this effect is not studied here.

1 The Deflagrative Cycle

In Fig. 2, a developed view of a typical ICWR is shown with stratified charging, radial inlet partition walls and dual-sided deflagrative combustion. In Table 1 the given valve timing sequence considers both radial and circumferential partitioning. Phases I, II, and III are analyzed in this study.

2 Computational Model

A two-dimensional model is developed to compute the transient flow and combustion efficiently, in a channel with circumferential partition walls. For rotors with narrow channels, sidewall effects may not be negligible, but require a three-dimensional time-consuming computation.

2.1 Passage Geometry and Grid. Dimensions of the wave rotor channel that is being studied are shown in Fig. 3, which are representative of existing test wave rotor designs published in the literature, Table 2.
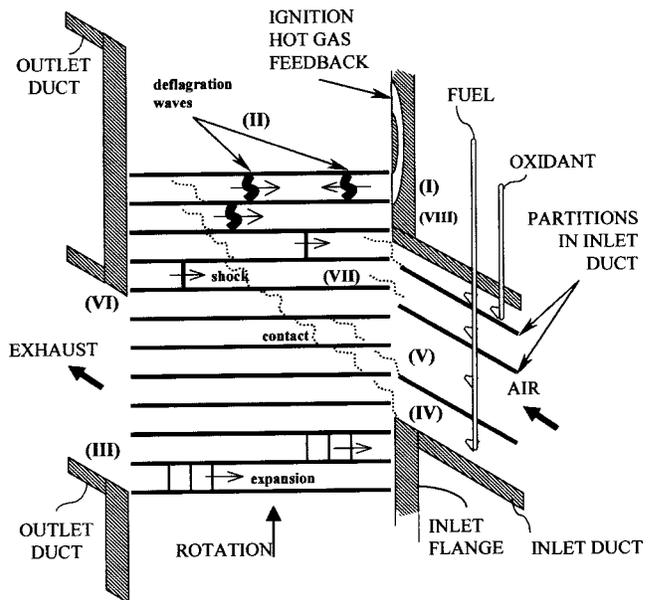
The total number of computational cells, including the solid cells of partition walls is 11,968, Fig. 4. The upper limit of grid aspect ratio is set to 9. Grid sensitivity tests showed no phase errors and differences are smaller than the variations, evaluated in this study, due to model assumptions.

2.2 Solver. Calculations are performed using the STAR-CD code, a general purpose, finite volume algorithm that operates on a versatile unstructured grid system to solve the conservation equations. Its modeling capability includes compressible, multiphase, and chemical reacting flows, through a choice of different Reynolds-averaged turbulent models, [16]. Extended versions of the SIMPLE [17] and PISO [18] algorithms are used for steady-state and transient calculations. Spatial differencing is second order, and a fully implicit first-order temporal differencing scheme is used.

For the presented results, normalized solver tolerances for all variables were set to 0.01, except 0.0001 for pressure. Convective terms for scalar equations are discretized with a blended upstream

Table 1 Proposed deflagration cycle

Phase	End (ms)	Description
I	0.065	hot gas injection (ignition)
II	3.865	constant volume combustion
III	4.585	exhaust port opens to turbine
IV	4.615	A little cold air is introduced from the pilot partition inlet to avoid pre-ignition. Lean fuel-air mixture is introduced from the remaining divisions of the inlet port (above and below the pilot partition).
V	4.815	Turbine exhaust continues. Lean mixture is introduced from all divisions of the inlet port.
VI	4.995	Exhaust port closed, shock-compression starts. Lean mixture inflow continues.
VII	5.055	Shock compression process continues. Richer mixture is introduced through the pilot partition inlet. Lean mixture inflows from the remaining divisions.
VIII	5.245	The richer pilot mixture continues to enter to the pilot partition. Cold-leakage control air is introduced into the remaining partitions. The initial mixture distribution is finally obtained.
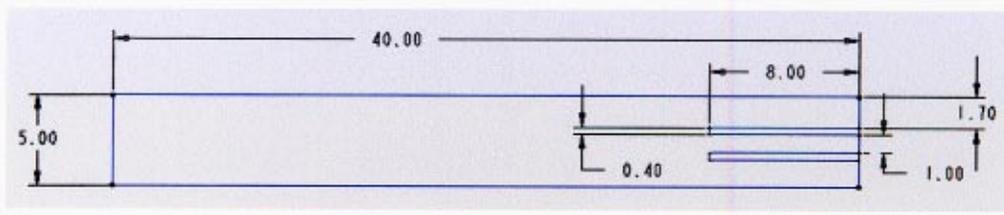
Fig. 3 Model dimensions (in cm)

and second order monotone advection and reconstruction scheme (MARS), for all other equations MARS scheme is employed. The total enthalpy form of the energy equation is solved with chemicothermal terms for scalars. For temperature and scalars a relaxation factor of 0.95 is used. The maximum Courant number was five times less than the solver allowance.

2.3 Turbulence. Intense turbulence is achievable and expected during the combustion period of a wave rotor, due to the immediately preceding high-speed inflow. The standard high Reynolds number k-ε model with algebraic law-of-the-wall functions is employed. This model has been used successfully in reactive flow studies with mixing and kinetics controlled conversion rate models, especially in internal combustion (IC) engines, [19,20]. It is valid only in the region of turbulent flow, where the local turbulent Re number ($\rho k^2/\mu\varepsilon$) is high. Despite the usual uncertainties involved in turbulent flows, useful results are being obtained, [21]. Model details can be found in [22,23]. Terms for compressibility and wall roughness effects are also present in the turbulence model used. Values assigned to model coefficients are given

Table 2 Selected internal combustor wave rotor specifications

	Nalim [4]	Bilgin [10]	Kentfield [15]	Nalim [29]	Current Study
Mean radius (cm)	8.15	N/A	9.53	25.8	N/A
Rotor length (cm)	15.24	40.6	25.4	60.6	40
Channel height (cm)	2.18	4.0	6.35	9.09	5.0
Cycles/second	560	N/A	100	191	190.7
Inlet area (cm^2)	26	16	10.6	-	N/A

Fig. 4 Computational grid in the partitioned region (closeup)

in Table 3. These values are similar to [24], where for cylindrical flames $C_{\varepsilon 2}$ is 1.79. The only notable change is in the turbulent Schmidt values of mixture fraction and mass fraction of fuel where slightly higher values are used compared to [24] and [25].

For k-ε models it is known that the prediction of swirling flows and recirculation zones is poor [20,26], compared to Reynolds stress equation models. Reynolds stress models (RSE) or higher-order closures can be used for simple geometries, however, in practical combustion devices less sophisticated representations have to be used because of computer capability limitations. For turbulent jet diffusion flames, [20], the superiority of RSE predictions is reported, together with the poor performance of the low Reynolds number models for the test case studied.

The turbulent time scale is in the order of one milliseconds and turbulence decays relatively quickly in the motionless channel regions. Turbulence that sustains combustion is generated by the jet-like partition exit flow. Thus the severity of the initial turbulence level in the fuel partition is critical for a high kinetic energy partition exit flow and subsequent high combustion rates.

For continuous flow devices, initial k and ε values can be estimated by making assumptions for turbulence intensity, T_i and characteristic length scale, l, [27]. However, for a charged wave rotor state with the inlet valve just closed, there is no internal mean velocity. For this reason, empirical estimates from spark ignited (SI) engine studies are employed. In these machines, the intake process generates a highly turbulent flow ($1.4 > u'/\bar{U} > 0.2$) that may persist throughout the compression phase, [28]. In the intake process of wave rotor engines the value of $u'/\bar{U}$ is probably smaller than that of the SI engines; however, intake $\bar{U}$ is high and the subsequent shock-compression process will intensify turbulence.

In Table 4, selected approaches for the estimation of initial turbulence level are summarized. Using these approaches, a total of eight different runs are performed with varying initial turbulent kinetic energy and dissipation rates, Table 5.

2.4 Boundary Conditions. The symmetry sidewall boundary conditions simulate a wave rotor channel with infinitely extending parallel hub and shroud walls. Much of the combustion takes place at constant volume, with inlet and outlet ends specified as solid walls. The turbine exhaust and subsequent mixture injection processes are specified by the use of pressure boundary conditions at inlet and outlet. Concentrations at outlet boundaries are

Table 3 Values assigned to standard k-ε turbulence model coefficients

	C_μ	σ_k	σ_ε	σ_h	σ_m	$C_{\varepsilon 1}$	$C_{\varepsilon 2}$	$C_{\varepsilon 3}$	σ_{fu}	σ_f	$C_{\varepsilon 4}$	K	E
Hjertager [24,25]	0.09	1.0	1.3	0.7	-	1.44	1.92	-	0.7	0.7	-	-	-
Hessel [46]	0.09	1.0	1.3	-	-	1.44	1.92	-1.0	-	-	-	-	-
Current study	0.09	1.0	1.22	0.9	0.9	1.44	1.92	0.0 1.44	0.9	0.9	0.33	0.42	9.0

Table 4 Initial turbulence level estimation via different relations. ($\tau_e = l/u'$ is eddy decay time, k_o and ε_o are the initial values.)

Estimate Source	Key Relations	k_o (m²/s²)	ε_o (m²/s³)	τ_e (ms)
Versteeg [27], general internal flows	$k = K \cdot (\bar{U} T_i)^2$ $\varepsilon = C_\mu^{3/4} \dfrac{k^{3/2}}{l}$ $K = 0.5 \sim 1.5$ $l = (0.07 \sim 0.1)L$	100 ($\bar{U}_i = 100$ m/s) ($T_i = 0.1$)	0.23e⁶ ($l = 0.7$ mm)	0.07
Tabaczynski [28], spark ignition engines	INTAKE: $u' \approx \bar{U}$ and $\varepsilon \approx (u')^3/l$ $l = 2 \sim 10$ mm TDC: $l \approx h$ h, chamber height	3600 ($\bar{U}_i = 60$ m/s)	7.10e⁶ ($l = 5$ mm)	0.7 at IVC
Abraham [19], premixed charge engine combustion	$k = \alpha(\eta_\nu \cdot \text{rpm})^2$ $\varepsilon = \beta(\eta_\nu \cdot \text{rpm})^3$ $\alpha = 0.608$ $\beta = 0.305$ $\eta_\nu = 40 \sim 60\%$ $1000 \sim 1500$ rpm	2.4e⁵	7.4e⁷	
Hessel [46], diesel engines at IVC	$k = C_k \bar{U}^2$ $\varepsilon = C_\varepsilon (\bar{U}^3/\sqrt{A})$ $C_k = 0.165$ $C_\varepsilon = 0.055$	590	2.4e⁶	
Kuo [40], port fuel injection engine at BTDC firing	$k = 0.9 \cdot \bar{U}_{\text{piston}}^2$ l is proportional to the closest wall distance	1.5e⁴ ($\bar{U}_i = 130$ m/s)	13.08e⁷	

first-order extrapolated. Hot gas injection is modeled by an inlet boundary, where the injection pressure is calculated from the specified values of density and temperature.

2.5 Turbulent Combustion Model. Combustion calculations implemented in quasi-steady one-dimensional wave rotor codes are quite developed, [9]. They are applied to practical test cases operating in different combustion modes, [8,29]. Multiple species or a single reaction progress variable is utilized to allow for a variable fuel-air ratio. Mixing controlled reaction is combined with a simple eddy diffusivity model. Other notable features that are incorporated are limit and combustion temperature factors and a simple total-energy based flammability limit, [9].

The turbulent combustion process in wave rotors resembles that of the internal combustion engines. For this reason models developed for SI and CI engines are believed to be applicable to wave rotor combustion phenomena. The conventional approach in modeling turbulent premixed combustion in SI engines is to use detailed chemistry or one-step irreversible Arrhenius kinetics for chemical combustion, combined with a mixing controlled conversion rate model, [19].

A brief review of the computational modeling alternatives are given in [26,30]. Among them, the presumed PDF and eddy breakup-type methods are two popular approaches for the closure of mean reaction rate. Both methods with sub-variants are being applied to a large range of industrial combustion problems [31]. For gas turbine combustion with sprays, the eddy breakup model has provided some useful results, [32]. Both methods, applied to a steady bluff-body stabilized burner resulted identical solutions irrespective of the turbulence model used, [20]. In [33], a modified form of the eddy breakup reaction rate equation is used to predict premixed flame propagation and damaging overpressures in large (2.5 m dia.) and long cylindrical vessels. Engine simulations in which the reaction rates are predicted by mixing-controlled combined models are numerous, [32,34,35].

In this study, turbulent combustion of propane (C_3H_8) is modeled via the eddy-dissipation model of Magnussen [24]. The model is applicable to both premixed and non-premixed systems. Other closely associated models are the transport and algebraic eddy break up models of Spalding [36]. The reaction time scale T_R is calculated as the sum of turbulent kinetic, k/ε and chemical kinetic, $\rho m_{lr}/R_{kin}$ time scales. This combined approach prevents over-prediction of reaction rates near wall regions. The fuel reaction rate then follows from Eq. (1).

$$R_F = \frac{\rho}{T_R} A_{\text{ebu}} \cdot \min\left[m_F, \frac{m_O}{s_O}, B_{\text{ebu}} \frac{m_P}{s_P} \right] \tag{1}$$

The eddy breakup coefficients A_{ebu} and B_{ebu} are used to control strength of the source. The absolute value of A_{ebu} can range between 2 to 10; the lower value is used if the reaction rate is controlled by the consumption of a reactant, and the higher, if by the rate of formation of a product. In this study 4 and 0.5 is used for A_{ebu} and B_{ebu}, respectively, which are the typical values used in the literature, [24,25]. In [37], a numerical method is proposed for the calculation of A_{ebu} explicitly as a function of the mean and standard deviation of mixture fraction PDF. Commonly accepted values may be in error up to two orders of magnitude, especially in the rich regions of the flame. Sensitivity studies for these constants need to be performed. The eddy breakup model with the

Table 5 Turbulent test case configurations. All cases have pilot partitions.

CASE	Equiv. Rat.	k_0 m²/s²	ε_0 m²/s³	T_{tb} (s) $= k_0/\varepsilon_0$
1b (base)	0.8	3600	7.1e⁶	0.507e⁻³
1bt1	0.8	40.5	23460	1.720e⁻³
1bt2	0.8	3.461	4584	0.760e⁻³
1bt3	0.8	1.5e⁴	13.08e⁷	0.110e⁻³
1bt4	0.8	3600	0.89e⁶	4.045e⁻³
1bt5	0.8	100	0.23e⁶	0.434e⁻³
1bt6	0.8	2.4e⁵	7.4e⁷	3.240e⁻³
1bt7	0.8	590	2.4e⁶	0.246e⁻³

Table 6 Rate constants $(K=A.\exp(B/T)$ **in** $m^3 (kg.mol)^{-1} s^{-1})$

	K	A	B
$N_2+O \overset{K_1}{\underset{K_{-1}}{\leftrightarrow}} NO+N$	K_1	$1.8e^{11}$	-38370
	K_{-1}	$3.8e^{10}$	-425
$N+O_2 \overset{K_2}{\underset{K_{-2}}{\leftrightarrow}} NO+O$	K_2	$1.8e^{7}$	-4680
	K_{-2}	$3.8e^{6}$	-20820
$N+OH \overset{K_3}{\underset{K_{-3}}{\leftrightarrow}} NO+H$	K_3	$7.1e^{10}$	-450
	K_{-3}	$1.7e^{11}$	-24560
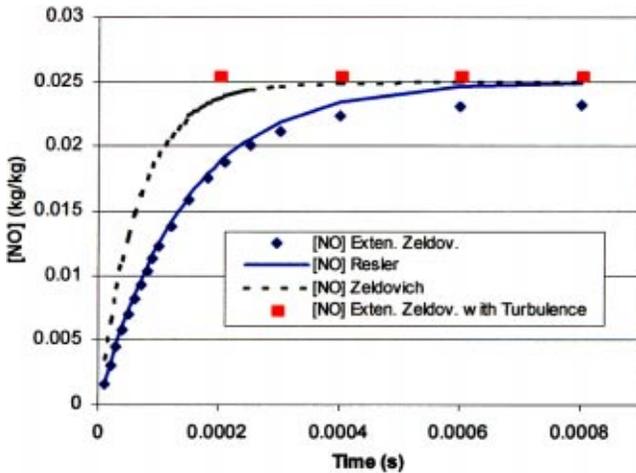
Fig. 5 Equilibrium and relaxation time comparisons of NO models

Table 7 Injected hot gas properties

Hot gas temperature $=2278$ K	Injection duration $=6.5e^{-5}$ s
Injection velocity $=750$ m/s	Density $=2.6532$ kg/m^3
Turb. kinetic energy $=1.500e^4$ m^2/s^2	Turb. dissipation $=1.308e^9$ m^2/s^3

Concentration (kg/kg)

$[C_3H_8]=0.0$	$[O_2]=0.0441$	$[CO_2]=0.1457$
$[H_2O]=0.0795$	$[N_2]=0.7307$	$[NO]=0.0$
[mixture fraction]$=0.0485619$		
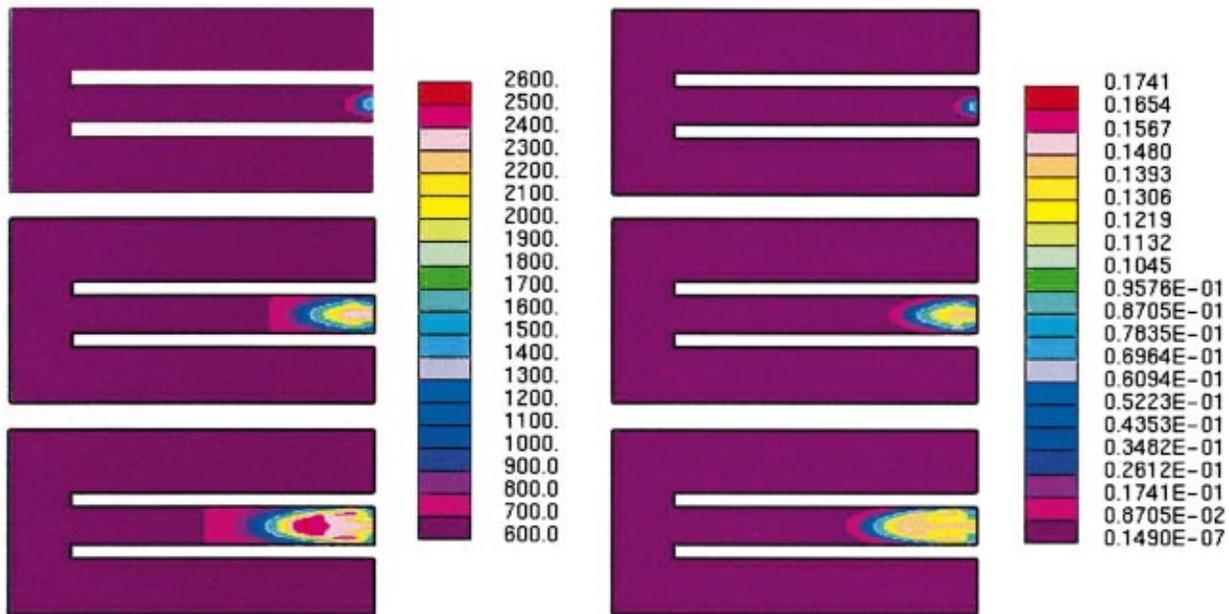
stated level of closure is reported, [38], to have some known drawbacks, notably in expressing convection by turbulence and turbulence generation.

A single step global reaction is assumed, where CO_2 and H_2O are produced in the background of N_2. R_{kin} is the reaction rate, which is calculated from chemical kinetics using an Arrhenius-type expression Eq. (2).

$$R_{kin(C_3H_8)}=-AM_{C_3H_8}T^{\beta}\left[\frac{\rho m_{C_3H_8}}{M_{C_3H_8}}\right]^m\left[\frac{\rho m_{O_2}}{M_{O_2}}\right]^n e^{-E_a/RT} \quad (2)$$

For propane, [39], constants in the rate expression (2) are $A=4.83e^9$ (kmol/m^3)$^{1-m-n}$, $\beta=0.0$, $E_a=1.26e^8$ (kmol/J), $m=0.1$, $n=1.65$. These kinetic constants, including the pressure dependency, can also be estimated by calibrating computed and measured laminar speeds over a range of equivalence ratios, pressures, and temperatures, [34,40].

2.6 NO_x Emission Model. NO_x emissions in SI and CI engines, propelled by the current environmental regulations are widely studied in literature. A wave rotor design for a high TIT gas turbine cycle with NO_x constraints has been done, [41], ignoring the NO_x formation and kinetics in the wave rotor component. For the selected deflagrative cycle, only the thermal NO production is taken into account, governed by the three extended Zeldovich steps, Table 6, [42,43]. Partial equilibrium assumptions are made to obtain the concentrations of radicals O, OH, and H, since they are not present in the combustion model.

NO history, obtained with this model, for a given temperature, and initial O_2 and N_2 concentrations, is compared in Fig. 5 with the two-equation Zeldovich [44] and Resler's [45] models. For this transient test case, the relaxation times of the extended Zeldovich mechanism and the later model are found to be matching.

The prompt and turbulent NO_x models, although being available, are postponed to the future work. The contribution of prompt NO becomes significant in rich flames only. Turbulence-chemistry interaction is expressible by the joint PDF of concentrations and temperature. For the transient equilibrium test case, Fig. 5, it is observed that the results are dependent to the number of PDF integration steps. For this reason turbulent contribution will not be included until a complete validation study is available.

Fig. 6 Temperature (K) (left) and CO$_2$ concentration (kg/kg) (right) during the hot gas injection phase. Time$=$5e-6, 4e-5, and 6.5e-5 s.
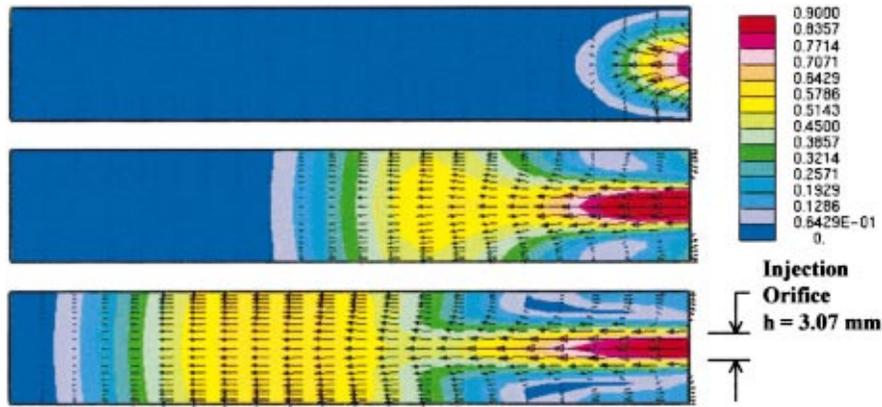
Fig. 7 Flow and Mach number in the fuel partition during the hot gas injection phase. Time=5e-6, 4e-5, and 6.5e-5 s.

3 The Ignition Phase

Two different methods of ignition are investigated. In one case, combustion is initiated in the so-called ignition cells, by specifying percent fuel burned during the ignition process and time it takes, [25]. Although simple to implement, this method resulted in unrealistically long ignition durations. This further decreased the rate of subsequent combustion due to rapidly decaying turbulence level in the channel.

Another approach is to use hot gas from previously combusted products to initiate combustion, which is one of the viable alternatives of the practical experimental wave rotor engines, [11,29]. In this study, hot gas, Table 7, is introduced to the computational domain from a small surface at the inlet, at a specified mass flow rate and chemical composition. Temperature, CO_2, and Mach number distributions at three time steps during this period are presented in Figs. 6, 7.

With these hot gas injection properties it became possible to obtain a partition exit flow that is close to the critical state, Mach number reaching to 1.0 as shown in Fig. 8. High speed flow at the partition exit is beneficial because of the corresponding penetration and high rate of turbulent energy production at the jet mixing layer, which in parallel increases the reaction rate in the channel, Fig. 9.

At this level, in ICWR engines, detailed ignition models are not attempted. However, future work can utilize fuel spray and special models implemented in existing codes for engine combustion, [40,46,47].

4 Initial Fuel Distribution in the Channel

Configurations with different initial fuel distributions can be achieved by stratification in the inlet duct.

Fig. 8 Mach number distribution of partition exit flow. Hot gas injection. Time=0.165 ms. (Refer to Fig. 7 for color map.)
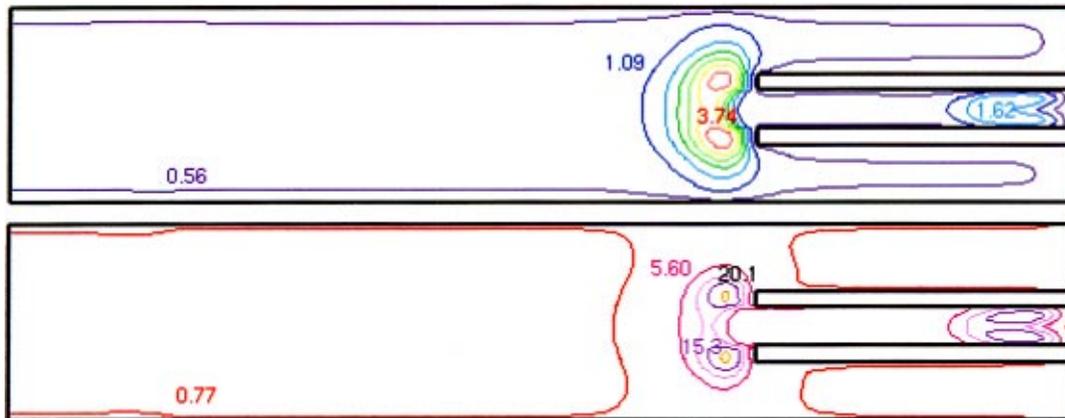
Fig. 9 Nondimensional turbulent kinetic energy (top) and dissipation (bottom) distributions of partition exit flow. Hot gas injection. Time=0.165 ms.

Fig. 10 Initial fuel distribution. Configurations are labeled (a), (b) and (c), from top to bottom.

The first configuration that was studied is shown in Fig. 10(a), where a stoichiometric fuel/air is specified between the pilot partition walls, and air with no fuel is present at the top and bottom partitions. The remaining part of the channel is filled with a lean fuel/air mixture of 0.8 equivalence ratio.

Compositions of the five-component mixture for sample equivalence ratios are presented in Table 8. For Configuration (a), it is found that due to the severity of the pilot partition exit flow, recirculation regions are developed near the tips of the partition walls. This flow structure abruptly quenched the combustion zone by convecting cold air from the buffer layers, Fig. 11. The reaction rate reduced considerably. For cases where pilot partition walls are not present the reaction rate is initially slow but there is no abrupt termination.

Decreasing the extent of the cold air buffer as shown in Fig. 10(b) has solved this problem. It is observed that, a fairly one-dimensional flame front propagates with high speed up to the middle of the channel. Approximately at the third millisecond, having slight variations in its value depending on the initial turbulence level and hot gas injection parameters, a sharp slowdown occurs in the combustion rate. The mean velocity in the constant-volume channel oscillates between zero and approximately 60 m/s, as the waves continuously reflected from the boundaries. Dissipation produced at the boundary layer is periodically convected away from walls, increasing reaction rate at core regions. If a considerably long time passes, this results in a ladder like shape in the fuel concentration distribution; a typical plot is shown in Fig. 12.

This slowing of the burning process, which can be associated with the rapidly decaying initial turbulence level in the channel, is not desirable in existing practical wave rotor configurations. In cycle designs studies, especially in long channels with turbulent flame speeds, combustion can be started also from the other channel end by hot combustion products, which normally remain from

Table 8 Initial mixture compositions (kg/kg) and stagnation conditions

Stagnation pressure=7.6e⁵ Pa Lean ($\Phi=0.8$)			Stagnation temperature=600 K Stoichiometric ($\Phi=1.0$)		
$[C_3H_8]=0.04856$	$[O_2]=0.22074$	$[CO_2]=0.0$	$[C_3H_8]=0.05997$	$[O_2]=0.21809$	$[CO_2]=0.0$
mix. frac=0.04856	$[N_2]=0.73068$	$[H_2O]=0.0$	mix. frac=0.05997	$[N_2]=0.72194$	$[H_2O]=0.0$
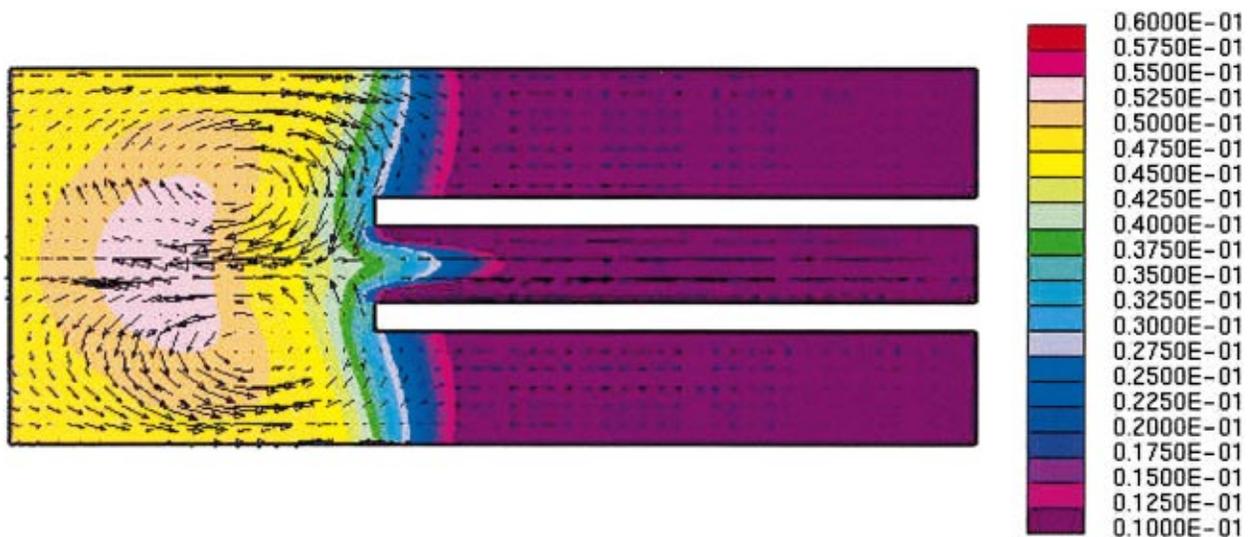
Fig. 11 Pilot fuel partition tip recirculation region. Velocity vectors and C_3H_8 (kg/kg) contours. (Ignition cells.) (Time =15.5 ms.)

Fig. 12 Fuel (C_3H_8) Concentration in the channel after a long time (10.1 ms). Refer to Fig. 11 for field plot color map.

the previous cycle, [4]. The dual initiation of combustion speeds the process, and initial charge can be consumed in a reasonable time.

Figure 10(*c*) shows the initial fuel and combustion products distribution for the dual ignition configuration. Compositions of combustion products will be discussed in Section 5.3. Their exact location is determined so that wave rotor channel contains the same amount of fuel as specified in [4] for the design operating conditions of the topped engine at the conditions given in Table 8. This final configuration is the starting point of the selected test cases that are presented in the next section.

5 Results

5.1 Initial Turbulence. In Fig. 13 total channel fuel mass histories are compared for the eight initial turbulence test cases. At the end of the fixed constant volume combustion period, there is approximately 20% variation in the remaining unburned fuel mass, if the extreme case, with unrealistically high turbulent kinetic energy and relatively low dissipation (Case t6), is excluded. As long as a representative trend is used, like the combustion parameters that are kept at their basic literature values, this variation will not affect the conclusions of this study, which focuses on specific design features to improve and quantify NO formation on a relative basis.

The turbulent time scale, which, due to the eddy dissipation model, is in the same order of the turbulent combustion rate, is changing in the course of combustion. Dissipation determines the

later values of turbulent kinetic energy. With a high initial dissipation, initial kinetic energy will die out rapidly, affecting the rate of combustion in later times. During startup, fuel mass consumption is high for the test cases with high initial turbulent kinetic energy. The latter variation is attributed to the flow and to the chemical kinetic time scale term in the reaction rate of the combustion model. It is also observed that resulting combustion front shapes were somewhat different for different initial turbulence levels.

For the NO computation results in this report, the empirical study of Tabaczynski [28] is utilized (Case 1b), since this model appears representative of all the fuel burn rate trends.

5.2 Test Cases. Test cases are selected to analyze NO_x production in the channel for different stratifications and compare the effects of partition, equivalence ratio and air buffer, Fig. 14.

Case (3), has the simplest charge distribution, with no stratification, with lean equivalence ratio. All partitioned cases have the cold air buffer near the hub/shroud inlet, resulting in nearly the same amount of initial fuel. For cases (2a), (2b), and (1g), without having pilot partition walls, it is not realistically possible to introduce such a sharp divided initial air buffer. These cases are studied only to understand separately the effect of fuel stratification and the effect of physical partitioning.

Cases (1f) and (1g) feature air-core region that reduces the remaining unburned fuel in the channel at the end of the constant volume combustion phase. These cases are designed to show the hypothetical limit of emission levels and combustion efficiency
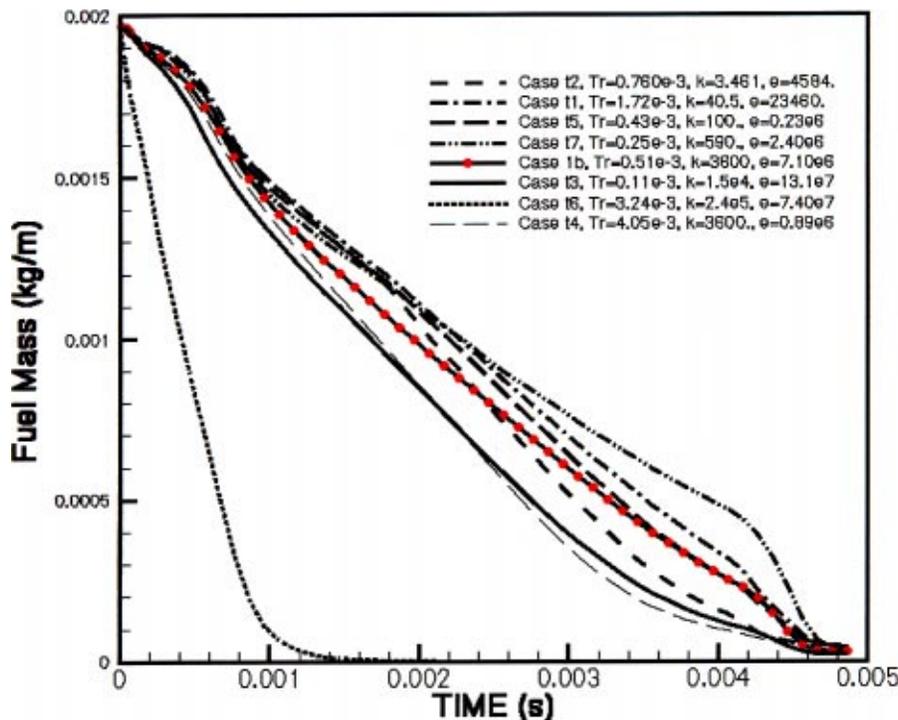
Fig. 13 Total fuel history in the channel for different initial turbulence levels. Dotted curve is specified in the computations.
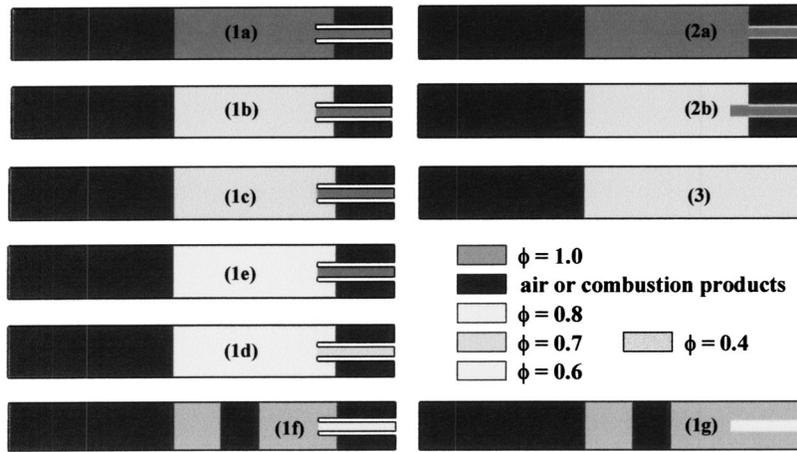
Fig. 14 Test cases studied. Initial fuel distribution. (See color key for equivalence ratios. Cases on left have partition walls).

that can be possible for the configuration and wave rotor cycle studied. Case (1g) does not have pilot partition walls and the air buffer region is not placed for comparison purposes, unlike Cases (2a) and (2b).

5.3 Combustion Products From Previous Cycle. The composition of combustion products that remained from the previous cycle is different for all cases. A reasonable estimate for the initial gas temperature and NO concentration is to use the constant enthalpy/pressure chemical equilibrium composition value and corresponding flame temperature. These parameters cannot be known exactly unless the converged periodic solution of the full cycle is available.

Sensitivity of results to the initial burned gas flame temperature is found to be high, especially for lean mixtures. For stoichiometric test cases with different initial combusted gas temperatures

and zero initial NO content, final NO levels at the end of combustion are similar, but having quite different histories, Fig. 15. Lean cases may aproach the same level after very long combustion times.

Compared to the initial equilibrium temperature, initial NO concentration in the channel has a slight effect on the final emission levels. In a global sense, different initial NO levels, with similar combusted gas flame temperatures, will converge as the combustion proceeds.

5.4 Primary Chamber Stoichiometry. Cases 1a, 1b, 1c, and 1e, all have pilot partition walls, with stoichiometric initial composition in the partition. Primary chamber region contains stoichiometric (1a) and lean mixtures with decreasing equivalence ratios (1b-0.8, 1c-0.7, 1e-0.6).

Figure 16 shows the overall NO concentration in the channel
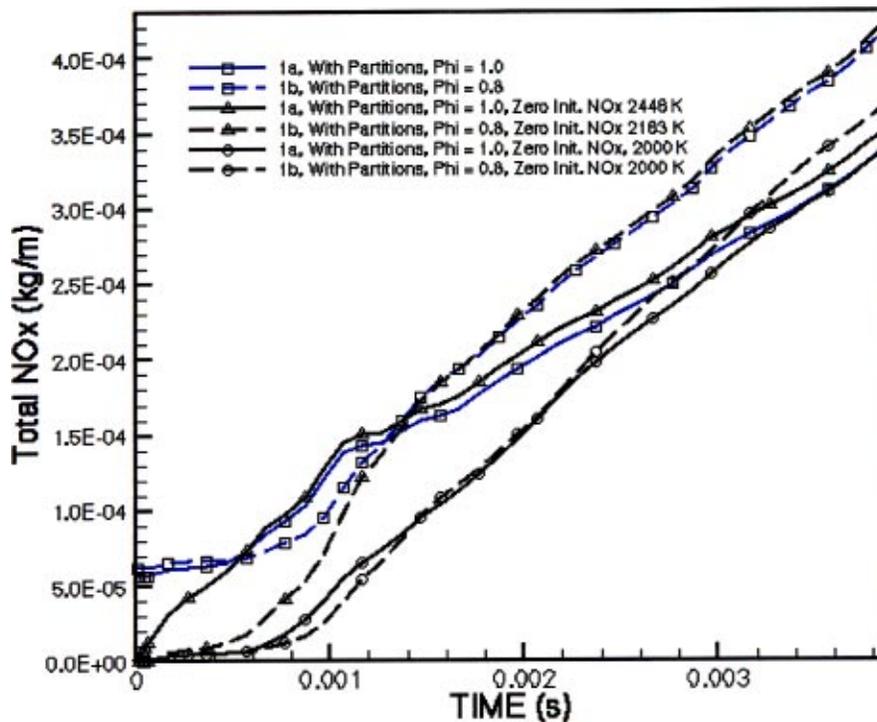
Fig. 15 Total NO mass versus time for different initial combusted gas temperatures and NO levels
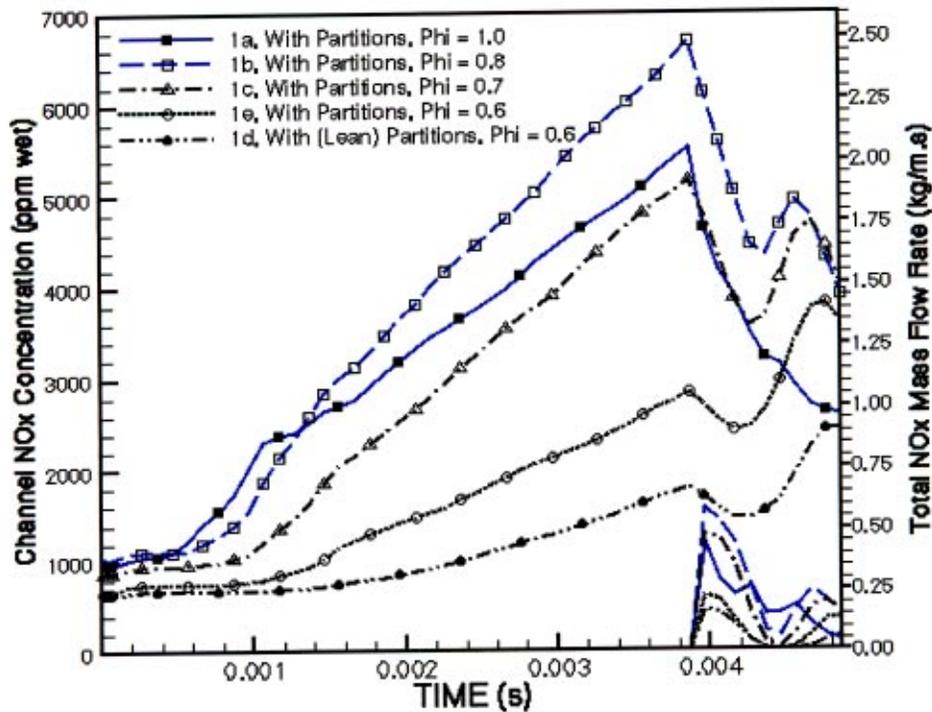
Fig. 16 Total NO$_x$ (ppm) versus time for cases (1a, 1b, 1c, 1e, 1d). (NO$_x$ mass flow through the exhaust port are plotted on lower right corner.)

vs. time for these cases. Wave rotor passage averaged NO concentration reaches its peak around equivalence ratio 0.8 and becomes lower for leaner test cases. This is an expected result in parallel with that of IC engine emission trends. The calculated overall NO$_x$ (ppm) levels are found to be higher than typical limits set by regulations and attained emissions of industrial gas turbines, again as expected.

The turbine exhaust starts at 3.865 ms. During this phase, for some time, NO concentration in the channel decreases. For stoichiometric burn case, this trend continues for the rest of the exhaust phase. But for all lean burn cases, NO concentration in the channel starts increasing again, and for the leanest case, exceeds the level reached at the end of combustion. The initial decrease is attributed to the high NO$_x$ convected by the outflow of previous cycle combustion products. The second peak is due to the relative magnitudes of the three main NO$_x$ sources; ongoing combustion process close to the partition tips, combustion process at the fuel rich mixture/hot products interface and NO$_x$ produced by the combustion products of the previous cycle due to increasing temperature.

For the lean case, the turbine exhaust phase ends and the outlet port is closed before the gas in the channel with high NO concentration reaches to the outlet port. See Fig. 16, where NO mass flow rates through the exhaust port are plotted at the lower right corner. The channel NO concentration begins increasing as the unburned fuel leaves the channel. During this phase of outflow, the channel loses very little NO, since only unburned fuel leaves. Moreover previous combustion products have already left, leaving only the highly expanded partition tip gas, as the sole NO source in the channel. Combustion and complex kinetics at the partition tip region is believed to be the cause, in spite of the temperature decrease due to the expansion wave, which should retard the NO production.

5.5 Effect of Partitions, Cases (1a, 1b, 2a, 2b, 3). Figure 17 shows the channel total fuel mass histories. Fuel consumption rate is higher for stoichiometric, compared to lean mixtures. How-

ever their difference disappears towards the end of constant volume combustion process. In (2a) and (2b), cold air buffer region is in direct contact with the stoichiometric fuel mixture. The fresh air buffer dilutes the combustion zone, and results in very low combustion rates and low NO concentrations, Fig. 18.

The other limiting configuration is the case with no air buffer and partition, Case 3. This case has resulted in the highest emission level of all the configurations studied, expected for a configuration with no possibility of cold air suction to the combustion zone. For Case 3, channel NO concentration peak that occurs during the exhaust phase is also the highest of all the configurations studied, Fig. 18.

Finally, during the exhaust phase, for cases without partition but with air buffer, total NO$_x$ concentration continuously decreases without changing its trend, Fig. 18.

5.6 Pilot Partition Stoichiometry, Cases (1d and 1e). Cases 1d and 1e both have same lean primary chamber composition, with 0.6 equivalence ratio. However in Case 1d, the fuel injection partition region has a leaner composition (with $\Phi = 0.8$) than Case (1e), which is stoichiometric. Referring to Figs. 16 and 17, lean fuel partitions case has slower overall reaction rate with a large quantity of remaining unburned fuel and corresponding low NO concentrations.

5.7 Lowest Emission Design, Cases (1f and 1g). The NO emission for a given engine is application dependent. Parameters like the power requirement, thrust level, specific fuel consumption, type of fuel, turbine inlet temperature limit, etc., influence the lowest available emission limits. A typical new aircraft research goal was the limit of 5 g/kg$_{fuel}$ set as a target of NASA's High Speed Civil Transport program. The emission standards set by the Environmental Protection Agency (EPA) depend on the engine's power output and intended use (utility or industrial). The typical NO$_x$ limit for industrial units with power outputs below 30 MW is 150 ppm (dry), [48]. For some geographic regions, for low
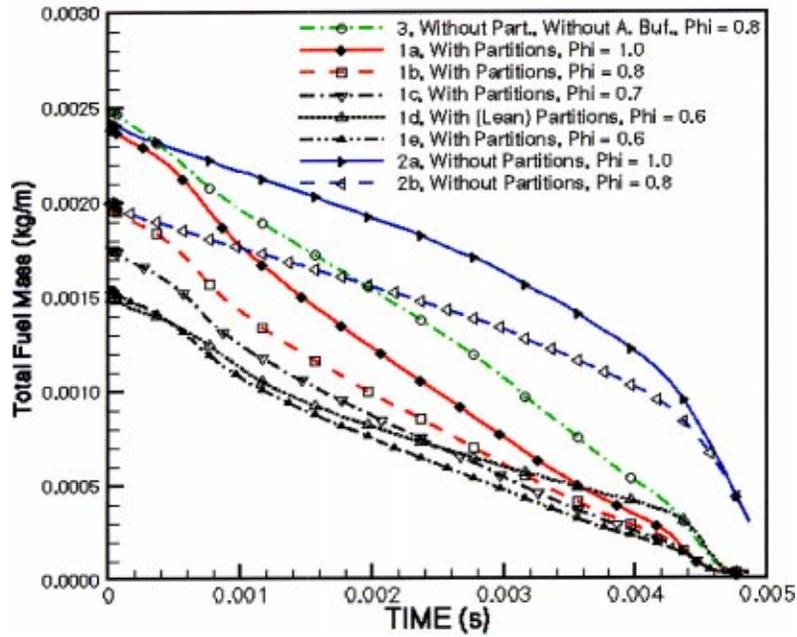
Fig. 17 Unburned fuel mass in the channel

power levels, NO_x limit has been set to 9 ppm (dry at 15% O_2), which is determined by considering the best available technology for gas turbine engines, [49].

For internal combustion wave rotor engines the best available technology is not yet known. For the concept studied in this report, configurations that produce lowest emissions can be designed. Cases (1f) and (1g) are specially selected to show the qualitative NO limits possible. The air core region of these cases reduces the overall fuel-air ratio considerably. Since for these test cases the resulting flame temperature is very low (T_{flame}(1f) $= 1390$ K, T_{flame}(1g) $= 1479$ K), initial equilibrium NO, that is contained only in the previous cycle combustion products, remains practically constant during the combustion.

For these cases the beneficial effect of partition walls to the combustion rate becomes more apparent compared to other cases, since as the average flame temperature drops, combustion rate depends more on turbulence than kinetics. In test Case (1g), which does not have pilot partitions, approximately half of the initial fuel remains unburned in the channel at the start of the turbine exhaust phase. On the other hand, due to the presence of partitions, in test Case (1f) remaining unburned fuel is comparable to other lean cases that are previously discussed.

Case (1f) can be considered as the lowest emission design that will lead to emission targets around 100 ppm, or under 1 g/kg_{fuel}. The goal of 10 ppm requires more detailed level of understanding.
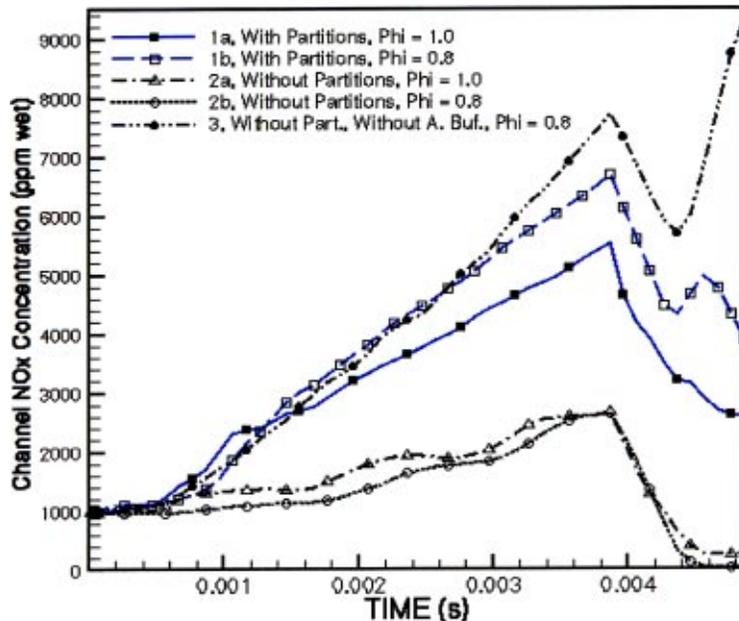
Fig. 18 Total NO_x (ppm) versus time for cases (1a, 1b, 2a, 2b, 3)
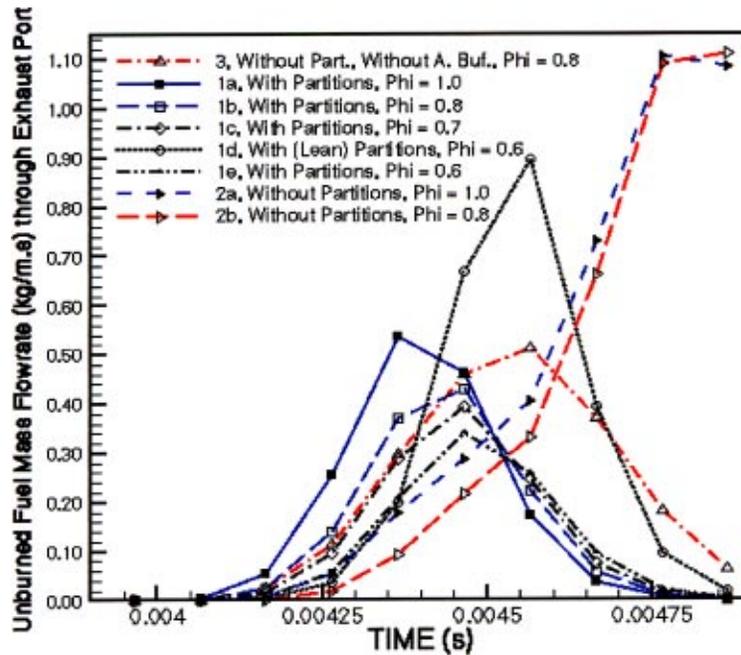
Fig. 19   Unburned fuel exhaust flow rate histories

These levels can be approached with lean premixed combustion but should be noted that additional kinetic mechanisms and interactions with turbulence will occur.

5.8 Turbine Inlet Compositions.   The mass flow rate averaged turbine inlet temperatures are not calculated. During exhaust, due to the expansion wave, combustion product's temperature decreases from 2500 K to 1900 K for Case (1c).

Fuel mass flow rate to the turbine during the exhaust phase is plotted in Fig. 19. The fuel spot, which remained from the uncompleted combustion, causes a fuel flux peak as it exhausts from the channel outlet.

The peaks in the instantaneous NO_x concentrations at the exhaust port, in Fig. 20, are due to the channel regions with different temperatures and compositions. Two primary peaks are clearly observed for lean burn configurations corresponding to two combustion zones, surrounding the unburned fuel. These two peaks are not very noticeable for the stoichiometric case. From a design point of view the magnitude of both peaks should be made equal and decreased.

Total ppm of NO exhausted to turbine can be calculated by a mass flow weighted time average. Corresponding values for the test cases are presented in Table 9.
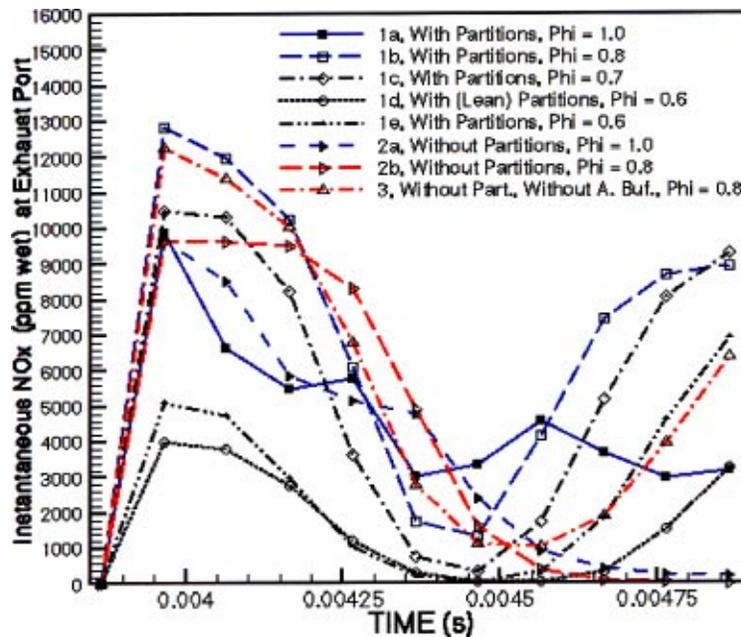
Fig. 20   Instantaneous exhaust NO_x concentrations (ppm wet)

Table 9 Emission indices (EI), mass weighted time-averaged turbine NO_x concentrations (ppm wet), and stagnation pressure rise ratio for combustion

Case	Fuel/Air Ratio	Average Pressure Rise	EI (kg/kg)	NO_x (ppm)	Configuration
1a	0.057	2.7	0.141	5100	(1.0) with partitions
1a_o	0.057	2.7	0.176	5300	zero initial NO, (1.0), with partitions
1b	0.046	2.5	0.216	7100	(0.8) with partitions
1b_o	0.046	2.5	0.257	7200	Zero initial NO, (0.8), with partitions
1c	0.041	2.4	0.185	5400	(0.7) with partitions
1e	0.035	2.2	0.108	2400	(0.6) with partitions
1d	0.035	2.0	0.070	1600	(0.6) with lean (0.8) partitions
1f	0.021	1.6	0.00106	220	Air core, with lean (0.6) partitions
1g	0.023	1.7	0.000378	300	Air core, without air buffer and partitions. With (0.6) fuel region
2a	0.058	2.1	0.094	3700	(1.0) Without partitions
2b	0.045	1.9	0.118	4200	(0.8) Without partitions
3	0.051	2.6	0.229	5700	(0.8) Without air buffer and partitions

6 Conclusions and Future Work

The use of pilot partition to boost the main chamber combustion, and air partitions, in avoiding hot gas leakage to the cavity is apparent. The drastic quenching effect of the air buffer limits the application of this concept, while its amount accurately controlled to cases with pilot partitions only.

Emission indices, calculated at the end of the constant volume combustion phase are tabulated in Table 9 (EI = (kg NO emitted)/(kg fuel burned)). For different configurations, calculated NO emission indices should be compared considering the percent reaction completed. For example "without partition and with air buffer" cases have the least emissions, since the overall chamber temperature had not had time for drastic NO production. Given more time, these cases will also reach or may exceed (as observed in Case 3) the highest emission levels of Table 9.

Since the remaining unburned and initial fuel amounts are different for each configuration, comparison of engine NO_x potential should be based on both the total ppm NO_x exhausted and emission index at the end of constant volume phase, Table 9. Note that Case 3, without partition and air buffer, has the highest emission index of all the configurations (excluding cases with no initial NO in the residual gas). However, because of the absence of partitions that increases the reaction rate, at the end of constant volume combustion, fuel burned is low thus the total ppm NO_x exhausted to turbine is low. The NO formed during a cycle and the NO emitted are not directly linked; a significant amount remains with the residual gas, and affects how much will be formed in the next cycle.

In this research, a particular method for obtaining low NO_x levels in internal combustor wave rotors is studied. As for other combustion devices there may be other design approaches not yet studied for wave machines. In conventional gas turbine combustors the common method for obtaining low emissions is the addition of more air into the primary combustion zone to lower the flame temperature, facilitate better mixing, and eliminate hot spots and reduction of combustor residence time. The stratified combustion approach that is studied here is the appropriate equivalent for non-continuous flow machines.

While comparing the emission levels that are stated in this report with other classes of machinery such as gas turbines and internal combustion engines, the specific application should be taken in to account. Most of the test cases in this study have very high fuel/air ratio compared to the existing applications. This re-

sults very high channel temperatures, high power output, and thus high emissions. Only the "limit" test Cases ((1f) and (1g)) have low fuel/air ratios like conventional engines, Table 9. In parallel, these cases have very low emission indices compared to other cases. The design of the lowest emission internal combustion wave rotor could be realized by a systematic development approach as has been done for conventional gas turbine combustors. A realistic target, perhaps a 10 ppm limit, may be set for wave rotor machines, however only after a 100 ppm engine has been successfully designed and built. For some preliminarily numerical test cases, it is shown in this report that engines close to the 100 ppm goal can be realized.

Recently, multistep reactions for rich combustion allowing fuel-rich pilot partition, [50], and radial leakage flow to the rotor cavity, [51], are studied for the same geometry. Future work may include different NO_x models, unsteady heat transfer, realization of the complete cycle described in Section 1 and comparisons with one-dimensional codes, and modeling rotor swirl in hot gas and fuel injection processes.

Acknowledgments

Nomenclature

A = Arrhenius constant
A = area
A_{ebu} = eddy breakup model constant
B_{ebu} = eddy breakup model constant
β = temperature exponent
E_a = activation energy
ε = dissipation
ϕ = equivalence ratio
h = chamber height
η_v = volumetric efficiency
k = turbulent kinetic energy
K = rate constants
l = turbulent length scale
L = characteristic length
m = mass fraction
M = molecular weight
R = gas constant
ρ = density
t = time
T = temperature
T_i = turbulent intensity
T_R = reaction time scale
T_{tb} = turbulent time scale
τ_e = eddy decay time
u' = fluctuating velocity component
$\bar{U}$ = average velocity
y^+ = nondimensional first cell distance

References

[1] Welch, G. E., Jones, S. M., and Paxson, D. E., 1997, "Wave Rotor Enhanced Gas Turbine Engines," ASME J. Eng. Gas Turbines Power, **119**(2), p. 469.
[2] Nalim, M. R., 1994, "Wave Cycle Design for Wave Rotor Engines with Limited Nitrogen Oxide Emissions," Ph.D. thesis, Cornell University, Ithaca, NY.
[3] Paxson, D. E., 1995, "A Numerical Model for Dynamic Wave Rotor Analysis," AIAA Paper No. 95-2800.
[4] Nalim, M. R., 1997, "Numerical Study of Stratified Charge Combustion in Wave Rotors," AIAA Paper No. 97-3141.
[5] Wilson, J., and Paxson, D. E., 1996, "Wave Rotor Optimization for Gas Turbine Engine Topping Cycles," J. Propul. Power, **12**(4), pp. 778–785.
[6] Welch, G. E., 1996, "Two-Dimensional Computational Model for Wave Rotor Flow Dynamics," Paper No. NASA TM-107192.
[7] Larosiliere, L. M., 1995, "Wave Rotor Charging Process: Effects of Gradual Opening and Rotation," J. Propul. Power, **11**(1), pp. 178–184.
[8] Nalim, M. R., 1999, "Assessment of Combustion Modes for Internal Combustion Wave Rotors," ASME J. Eng. Gas Turbines Power, **121**(2), pp. 265–271.

[9] Nalim, M. R., 2000, "Longitudinally Stratified Combustion in Wave Rotors," J. Propul. Power, **16**(3), pp. 1060–1068.

[10] Bilgin, M., Keller, J. J., and Breidenal, R. E., 1998, "Ignition and Flame Propagation Process With Rotating Hot Jets in a Simulated Wave Engine Test Cell," AIAA Paper No. 98-3399.

[11] Paxson, D. E., 1993, "A Comparison Between Numerically Modeled and Experimentally Measured Loss Mechanisms in Wave Rotors," Paper No. AIAA-93-2522.

[12] Jones, S. M., and Welch, C., 1996, "Performance Benefits for Wave Rotor Topped Gas Turbine Engines," Paper No. NASA TM-107193.

[13] Paxson, D. E., 1996, "A Numerical Investigation of the Start-Up Transient in a Wave Rotor," Paper No. NASA TM-107196.

[14] Paxson, D. E., 1996, "Numerical Simulation of Dynamic Wave Rotor Performance," J. Propul. Power, **12**(5), pp. 949–957.

[15] Kentfield, J. A. C., 1998, "Circumferential Wave Dividers in Wave-Rotors," Paper No. AIAA-98-3397.

[16] Freitas, C. J., 1995, "Perspective: Selected Benchmarks From Commercial CFD Codes," ASME J. Fluids Eng., **117**, pp. 208–218.

[17] Patankar, S. V., and Spalding, D. B., 1972, "A Calculation Procedure for Heat Mass and Momentum Transfer in Three Dimensional Parabolic Flows," Int. J. Heat Mass Transfer, **15**, pp. 1787–1806.

[18] Issa, R. I., 1986, "Solution of the Implicitly Discretised Fluid Flow Equations by Operator Splitting," J. Comput. Phys., **62**, pp. 40–65.

[19] Abraham, J., Bracco, F. V., and Reitz, R. D., 1985, "Comparisons of Computed and Measured Premixed Charge Engine Combustion," Combust. Flame, **60**, pp. 309–322.

[20] Gran, I. R., Ertesvag, I. S., and Magnussen, B. F., 1997, "Influence of Turbulence Modeling on Predictions of Turbulent Combustion," AIAA J., **35**(1), pp. 106–110.

[21] Abraham, et al., 1988, "Pressure Non-uniformity and Mixing Characteristics in Stratified Charge Rotary Engine Combustion," SAE Technical Paper No. 880624.

[22] El Tahry, S. H., 1983, "k-ε Equation For Compressible Reciprocating Engine Flows," J. Energy, **4**, pp. 345–353.

[23] Launder, B. E., and Spalding, D. B., 1974, "The Numerical Computation of Turbulent Flow," Comput. Methods Appl. Mech. Eng., **3**, p. 269.

[24] Magnussen, B. F., and Hjertager, B. H., 1976, "On Mathematical Modeling of Turbulent Combustion With Special Emphasis on Soot Formation and Combustion," *16th Symposium on Combustion*, The Combustion Institute, Pittsburgh, PA, pp. 719–729.

[25] Hjertager, B. H., 1982, "Simulation of Transient Compressible Turbulent Reactive Flows," Combust. Sci. Technol., **27**, pp. 159–170.

[26] Pope, S. B., 1990, "Computations of Turbulent Combustion: Progress and Challenges," *23rd Symposium on Combustion*, The Combustion Institute, Pittsburgh, PA.

[27] Versteeg, H. K., and Malalasekera, W., 1995, *An Introduction to Computational Fluid Dynamics—The Finite Volume Method*, Longman, London.

[28] Tabaczynski, R. J., 1976, "Turbulence and Turbulent Combustion in Spark Ignition Engines," Prog. Energy Combust. Sci., **2**, pp. 143–165.

[29] Nalim, R. M., and Jules, K., 1998, "Pulse Combustion and Wave Rotors for High-Speed Propulsion Engines," Paper No. AIAA-98-1614.

[30] Lau, J. H. W., 1995, "Comparison of PDF and Eddy-Dissipation Combustion Models Applied to a Propane Jet Flame," Combust. Flame, **102**, pp. 209–215.

[31] Libby, P. A., and Williams, F. A., 1980, "Turbulent Reacting Flows," *Topics in Applied Physics*, Vol. 44, Springer-Verlag, New York.

[32] Raju, M. S., 1992, "Heat Transfer and Performance Characteristics of a Dual-Ignition Wankel Engine," SAE Technical Paper No. 920303.

[33] Catlin, C. A., Fairwheather, M., and Ibrahim, S. S., 1995, "Predictions of Turbulent, Premixed Flame Propagation in Explosion Tubes," Combust. Flame, **102**, pp. 115–128.

[34] Kuo, T. W., and Reitz, R. D., 1989, "Computation of Premixed-Charge Combustion in Pancake and Pent-Roof Engines," SAE Technical Paper No. 890670.

[35] Kong, S., Han, Z., and Reitz, R. D., 1995, "The Development and Application of a Diesel Ignition and Combustion Model for Multidimensional Engine Simulations," SAE Technical Paper No. 950278.

[36] Spalding, D. B., 1971, "Mixing and Chemical Reaction in Steady Confined Turbulent Flames," *13th Symposium on Combustion*, The Combustion Institute, Pittsburgh, PA.

[37] Brizuela, E. A., and Bilger, R. W., 1996, "On the Eddy Break-up Coefficient," Combust. Flame, **104**, pp. 208–212.

[38] Hulek, T., and Lindstedt, R. P., 1996, "Computations of Steady-State and Transient Premixed Turbulent Flames Using PDF Methods," Combust. Flame, **104**, pp. 481–504.

[39] Westbrook, C. K., and Dryer, F. L., 1981, "Simplified Reaction Mechanisms for the Oxidation of Hydrocarbon Fuels in Flames," Combust. Sci. Technol., **27**, pp. 31–43.

[40] Kuo, T., 1992, "Multidimensional Port-and-Cylinder Gas Flow, Fuel Spray, and Combustion Calculations for a Port-Fuel-Injection Engine," SAE Technical Paper No. 920515.

[41] Nalim, M. R., Moscari, J. C., and Resler, L., 1993, "Wave Cycle Design for NO$_x$ Limited Wave Rotor Core Engines for High Speed Propulsion," ASME Paper No. 93-GT-426.

[42] Flowers, W. L., Hanson, R. K., and Kruger, C. H., 1975, "Kinetics of the Reaction of Nitric Oxide with Hydrogen," *15th Symposium on Combustion*, The Combustion Institute, Pittsburgh, PA, p. 823.

[43] Monat, J. P., Hanson, R. K., and Kruger, C. H., 1979, "Shock Tube Determination of the Rate Coefficient for the Reaction $N_2 + O \rightarrow NO + O$," *17th Symposium on Combustion*, The Combustion Institute, Pittsburgh, PA, p. 543.

[44] Zeldovich, B., and Raizer, P., 1966, *Physics of Shock Waves and High-Temperature Hydrodynamic Phenomena*, Vol. 1, Academic Press, San Diego, CA.

[45] Nalim, M. R., 1985, "NO$_x$ Control in Natural Gas Engines Using Exhaust Gas Recirculation," M. Sc. thesis, Cornell University, Ithaca, NY.

[46] Hessel, R. P., and Ruthland, C. J., 1995, "Intake Flow Modeling in a Four-Stroke Diesel Using KIVA-3," J. Propul. Power, **11**(2), pp. 378–384.

[47] Kong, S., Han, Z., and Reitz, R. D., 1995, "The Development and Application of a Diesel Ignition and Combustion Model for Multidimensional Engine Simulations," SAE Technical Paper No. 950278.

[48] Lefebvre, H. A., 1999, *Gas Turbine Combustion*, Taylor and Francis, London.

[49] Correa, S. M., 1992, "A Review of NO$_x$ Formation Under Gas Turbine Combustion Conditions," Combust. Sci. Technol., **87**, pp. 329–362.

[50] Pekkan, K., and Nalim, R., 2002, "On Alternative Models for Internal Combustor Wave Rotor Simulation," Spring Technical Meeting of the Central States Section, Knoxville, TN.

[51] Pekkan, K., and Nalim, R., 2002, "Control of Fuel and Hot-Gas Leakage in a Stratified Internal Combustion Wave Rotor," Paper No. AIAA-2002-4067.